JACS
JOURNAL OF THE AMERICAN CHEMICAL SOCIETY
Article
pubs.acs.org/JACS

Bidirectional Electron Transfer Capability in Phthalocyanine–$Sc_3N@I_h–C_{80}$ Complexes

Olga Trukhina,[†,‡] Marc Rudolf,[§] Giovanni Bottari,[†,‡] Takeshi Akasaka,[*,∥] Luis Echegoyen,[*,‡] Tomas Torres,[*,†,‡] and Dirk M. Guldi[*,§]

[†]Department of Organic Chemistry, Universidad Autónoma de Madrid, Cantoblanco, 28049 Madrid, Spain
[‡]IMDEA Nanociencia, Faraday 9, 28049 Madrid, Spain
[§]Department of Chemistry and Pharmacy and Interdisciplinary Center for Molecular Materials (ICMM), Friedrich-Alexander-Universität Erlangen-Nürnberg, 91058 Erlangen, Germany
[∥]Department of Chemistry, Tokyo Gakugei University, Koganei, Tokyo 184-8501, Japan
[⊥]Department of Chemistry, University of Texas at El Paso, El Paso, Texas 79968, United States

Supporting Information

ABSTRACT: To activate oxidative and/or reductive electron transfer reactions, *N*-pyridyl-substituted $Sc_3N@I_h–C_{80}$ (**4**) and C_{60} (**3**) fulleropyrrolidines have been prepared and axially coordinated to electron-rich (**1**) or electron-deficient (**2**) Zn(II)phthalocyanines (Zn(II)Pcs) through zinc-pyridyl, metal–ligand coordination affording a full-fledged family of electron donor–acceptor ensembles. An arsenal of photophysical assays as they were carried out with, for example, **1**/**4** and **2**/**4** show unambiguously that a Zn(II)Pc-to-$Sc_3N@I_h–C_{80}$ photoinduced electron transfer takes place in the former ensemble, whereas a $Sc_3N@I_h–C_{80}$-to-Zn(II)Pc electron transfer occurs in the latter ensemble. To the best of our knowledge, this is the first time that a fullerene-based molecular building block shows an electron transfer dichotomy, namely acting both as electron-acceptor or electron-donor, and its outcome is simply governed by the electronic nature of its counterpart. In light of the latter, the present work, which involves the use of $Sc_3N@I_h–C_{80}$, one of the most abundant and easy-to-purify endohedral metallofullerenes, is, on one hand, a paradigmatic change and, on the other hand, an important milestone *en-route* toward the construction of easy-to-prepare molecular materials featuring switchable electron transfer reactivity.

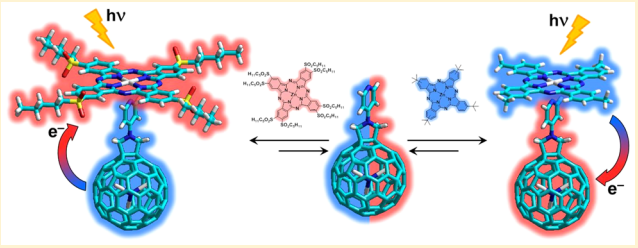

INTRODUCTION

During the last two decades, a significant effort has been made by the scientific community toward the preparation and study of electron donor–acceptor (D–A) ensembles exhibiting photoinduced charge separation, a fundamental process common to both natural photosynthesis and solar energy conversion, which stands out as one of the hot topics in contemporary science.[1] Among the molecular species used for this purpose, fullerenes (empty and endohedral) have been rapidly identified as some of the most promising candidates by virtue of their unique physicochemical properties. More precisely, empty fullerenes possess remarkable electron-acceptor properties,[2] which coupled with their small reorganization energy and their ability to promote ultrafast charge separation and slow charge recombination, have promoted the incorporation of these spherical nanostructures in systems where photoinduced electron transfer (PET) processes and solar energy conversion are sought.[3] However, a limitation of this family of fullerenes is the impossibility to significantly modify their electron-accepting or -donating features. Despite the large number of fullerene-based D–A conjugates that have been prepared, prompted by important advances in the chemistry of fullerenes functionalization,[4] exohedral derivatization of these empty carbon cages with a wide variety of photo- and/or redox-active moieties does not usually lead to an inversion in the direction of the charge transfer process. In these systems, the fullerene generally acts as the electron-accepting unit with only a few exceptions for which the carbon nanostructure behaves as the electron-donating moiety.[5]

On the contrary, endohedral metallofullerenes (EMFs), carbon cages that encapsulate atoms, ions, or clusters, possess a redox chemistry that, differently from their empty analogues, significantly varies as a function of the encapsulated species.[6] Moreover, EMFs exhibit higher absorption coefficients in the visible region of the electromagnetic spectrum and reduced HOMO–LUMO gaps compared to empty fullerenes, which make EMFs excellent candidates for optoelectronic applications. The initial reports documented the use of EMFs as electron-accepting moieties in covalently linked D–A systems,[7] but more recently, a few examples of EMF-based, D–A conjugates have been reported in which the EMF acts as an

Received: June 29, 2015
Published: September 24, 2015

DOI: 10.1021/jacs.5b06454
J. Am. Chem. Soc. 2015, 137, 12914–12922

electron-donor when covalently linked to electron-accepting moieties such as subphthalocyanines,[8a] perylene-diimides[8b,c] and tetracyanoanthraquinodimehane.[8d] Interestingly, for two of these EMFs, namely $La_2@I_h$–C_{80}[7b,8d] and $Lu_3N@I_h$–C_{80},[7c,8b] both reductive and oxidative PET processes have been observed upon covalently linking the EMF moiety to the appropriate redox-active unit.

Supramolecular interactions have also been used to construct D–A EMF-based architectures. This strategy offers important advantages with respect to the covalent approach such as the possibility to prepare and study a large number of systems through the rational combination of a given array of redox and/or photoactive molecules. Using self-assembly, supramolecular constructs have been prepared in which EMFs act either as electron-acceptor ($La_2@I_h$–C_{80}[9a] and $Li^+@C_{60}$)[9b] or -donor ($M_3N@I_h$–C_{80}; M = Lu or Sc)[9c] moieties. However, to the best of our knowledge, no examples of bidirectional PET have been reported thus far for D–A supramolecular ensembles comprising an identical fullerene species showing a dual electronic behavior, as previously observed for cyclo[8]-pyrrole-based supramolecular systems.[10]

RESULTS AND DISCUSSION

To achieve this goal, a $Sc_3N@I_h$–C_{80} derivative (**4**) was prepared and connected to an electron-donating (**1**) or an electron-accepting (**2**) Zn(II) phthalocyanine (Pc) by metal–ligand, axial coordination of the pyridyl moiety of the fulleropyrrolidine to the zinc metal center in the Pc macrocycle (Figure 1). Similarly, a pyridyl-substituted C_{60} derivative (**3**)

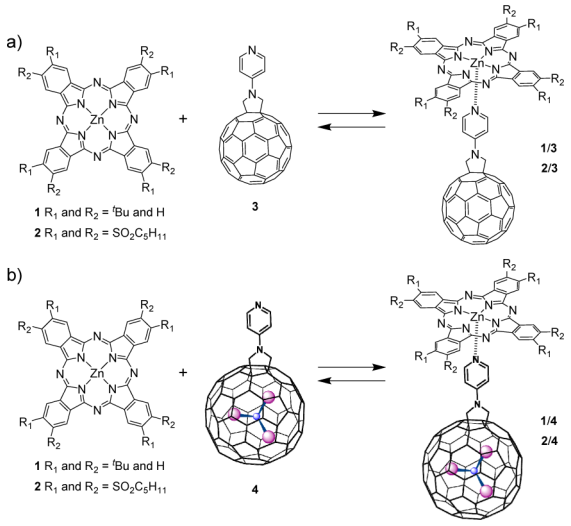

Figure 1. Metal–ligand, axial coordination of *N*-(*p*-pyridyl)-substituted fulleropyrrolidines **3** (a) or **4** (b) to Zn(II)Pcs **1** and **2** leading to supramolecular complexes **1**/**3** and **2**/**3**, and **1**/**4** and **2**/**4**.

was synthesized and axially coordinated to Zn(II)Pcs **1** and **2**. The choice of Zn(II)Pcs as supramolecular "counterparts" of **3** and **4** was prompted by several reasons. Pcs are aromatic macrocycles which possess excellent light-harvesting capabilities, good thermal stability, and rich redox chemistry.[11] Moreover, and importantly, the optical and electrical properties of these macrocycles can be easily modulated by the careful choice of the metal center and/or the peripheral substituents making them perfect building blocks for light harvesting, photovoltaic, and molecular photonic applications.[12] Time-resolved photophysical studies conducted with supramolecular assemblies **1**/**3**, **2**/**3**, **1**/**4**, and **2**/**4** revealed significant differences in the deactivation of the photogenerated Zn(II)Pc excited state. Whereas in the case of the complexes between Zn(II)Pc **1** and fullerene derivatives **3** or **4**, PET from the Zn(II)Pc macrocycle to the fullerene moiety dominates the deactivation dynamics, a $Sc_3N@I_h$–C_{80}-to-Zn(II)Pc charge transfer is observed for complex **2**/**4**, while no evidence of electron transfer was observed for complex **2**/**3**, in perfect agreement with electrochemical results obtained for derivatives **1**–**4**. Remarkably, in the case of supramolecular complexes **1**/**4** and **2**/**4**, a switchable PET process is observed involving, for the first time, a fullerene-based molecule (**4**), which acts both as electron-acceptor or electron-donor as a function of the electronic nature of its supramolecular counterpart. Additionally, and importantly, this work involves, for the first time, the use of $Sc_3N@I_h$–C_{80} as an electron-accepting/-donating redox moiety, an EMF which can be prepared[13] and separated in bulk quantities by non-HPLC methods[14] with a yield higher than C_{84}, the third most abundant empty fullerene.[15]

Octakis-(pentylsulfonyl) Zn(II)Pc **2** was prepared in 54% yield by the cyclotetramerization reaction of 1,2-dicyano-4,5-bis(pentylsulfonyl)benzene in a DMF/*o*-dichlorobenzene (*o*-DCB) mixture at 145 °C in the presence of zinc(II) acetate and characterized by mass spectrometry, electrochemistry, and UV–vis and NMR spectroscopies (Figures S5, S9, S15, S16). Tetra-*tert*-butyl Zn(II)Pc **1** was purchased from Aldrich. On the other hand, pyridyl-substituted fulleropyrrolidines **3**[16] and **4** were prepared by the 1,3-dipolar cycloaddition of an azomethyne ylide, generated *in situ* by the reaction of *N*-pyridylglycine and paraformaldehyde, to C_{60} and $Sc_3N@I_h$–C_{80}, respectively, in refluxing *o*-DCB under an argon atmosphere. Whereas the 1,3-cycloaddition of the as-formed azomethyne ylide to C_{60} occurs exclusively at a [6,6]-carbon bond leading to the formation of a single species, in the case of $Sc_3N@I_h$–C_{80}, two possible regioisomers resulting from the azomethyne ylide addition at a [5,6]- or [6,6]-carbon bond of the EMF sphere are theoretically possible. In this connection, monitoring the progress of the reaction leading to $Sc_3N@I_h$–C_{80} derivative **4**, the concomitant formation of both a [5,6]- and a [6,6]-regioisomers was observed at the early stages of the Prato reaction (Figures S1, S8). An aliquot of this reaction taken after 30 min shows an 83/17 ratio between the kinetic [6,6]-adduct and the thermodynamic [5,6]-adduct **4** (Figures S1, S2).[17] Interestingly, the [6,6]-adduct is fully converted to the more stable [5,6]-adduct **4** after 12 h in refluxing *o*-DCB in an isomerization process involving the pirouetting of the pyrrolidine addend (Figures S1, S2).[18] To the best of our knowledge, this is the second time a [6,6]-adduct generated by 1,3-dipolar cycloaddition of an azomethyne ylide to $Sc_3N@I_h$–C_{80} has been observed and characterized.[19] Column chromatography of the reaction crude on silica gel was carried out after 12 h, resulting in the isolation of the [5,6]-isomer **4** in a 12% yield as the only monoadduct, and negligible amounts of bisadducts.[20] $Sc_3N@I_h$–C_{80} derivative **4** was characterized by NMR and UV–vis spectroscopies, and mass spectrometry (Figures S3, S6, S14, S16). The MALDI-TOF spectrum of derivative **4** shows a major peak at 1228.9 *m*/*z* corresponding to the molecular ion, together with some small peaks at lower intensities due to fragmentation (Figure S3). The ^{1}H NMR spectrum of **4** in a CS_2/CD_2Cl_2 mixture shows two sets of doublets for both the pyridyl protons (8.44 and 6.91 ppm) and the two diastereotopic geminal protons of the pyrrolidine ring

DOI: 10.1021/jacs.5b06454
J. Am. Chem. Soc. 2015, 137, 12914–12922

Table 1. Redox Potentials of Derivatives 1−4 and Pristine $Sc_3N@I_h-C_{80}$ Obtained by DPVs, E_p vs Fc/Fc^+, *V*

compound	E_p^4 (red)	E_p^3 (red)	E_p^2 (red)	E_p^1 (red)	E_p^1 (ox)	E_p^2 (ox)
1	-	-	−1.81	−1.50	+0.16	+0.82
2[a]	−1.24	−1.06	−0.70	−0.65	+0.77	-
3	−2.46	−2.02	−1.51	−1.12	+0.89	+1.09
4	−2.58	−2.15	−1.43	−1.04	+0.29	+0.94
pristine $Sc_3N@I_h-C_{80}$[7d]	-	−2.37	−1.62	−1.26	+0.59	+1.09

[a]Only the first four reductions of octasulfonyl Zn(II)Pc **2** are reported.

(4.98 and 3.82 ppm) (Figure S6). As expected for a [5,6]-addition to $Sc_3N@I_h-C_{80}$, these latter protons show (i) cross-peak correlation to the same pyrrolidine methylene carbon atom at 62.6 ppm as inferred by $^1H-^{13}C$ HSQC NMR (Figure S11),[21] and (ii) a large chemical shift difference between them which arises from the different magnetic environments experienced by the two methylene protons (Figure S12) and the shielding of the *α*-methylene protons caused by the *trans*-lone pairs of the pyrrolidine nitrogen atom, according to Dorn et al.[22] Moreover, both geminal protons' resonance is downfield shifted by almost 1 ppm with respect to the chemical shift of the same geminal pyrrolidine protons in *N*-methyl-3,4-[5,6]-$Sc_3N@I_h-C_{80}$ fulleropyrrolidine.[22] This shift is probably due to a decreased ring current in **4** caused by the presence of the pyridyl unit.

The electrochemical properties of **1**−**4** and pristine $Sc_3N@I_h-C_{80}$ fullerene were investigated by cyclic voltammetry (CV) and differential pulse voltammetry (DPV) in *o*-DCB containing *n*-Bu_4NPF_6 (0.05 M) (Figures S16, S17) and their corresponding redox potentials are summarized in Table 1. In the case of *N*-(*p*-pyridyl)-(3,4)-fulleropyrrolidines **3** and **4**, up to four reduction and two oxidation peaks are observed. More specifically, C_{60} derivative **3** displays four reversible reduction peaks at −1.12, −1.51, −2.02, −2.46 V, and two irreversible oxidation peaks at +0.89 and +1.09 V, in agreement with previous reports.[16] Similarly, **4** reveals reversible reduction peaks at −1.04, −1.43, −2.15, and −2.58 V, a reversibility which is characteristic for [5,6]-$Sc_3N@I_h-C_{80}$ fulleropyrrolidine adducts.[23] In the anodic scan, **4** displays two quasi-reversible oxidation processes at +0.29 and +0.94 V. The former is ascribed to the oxidation of the I_h-C_{80} cage.[7d] It is interesting to note that **4** shows both the first reduction and oxidation shifted toward more positive and negative potentials, respectively, with respect to C_{60} derivative **3** (80 and 600 mV, respectively) and pristine $Sc_3N@I_h-C_{80}$ (220 and 300 mV). Considering the good electron-accepting and electron-donating features of derivative **4**, a possible electronic duality of this fulleropyrrolidine in PET reactions was anticipated (vide infra). A study of the redox properties of Zn(II)Pcs **1** and **2** was also conducted. In this context, whereas **1** shows two quasi-reversible reductions at −1.50 and −1.81 V and two quasi-reversible oxidations at +0.16 and +0.82 V, Zn(II)Pc **2**, featuring eight sulfonyl groups, shows seven anodically shifted, irreversible reduction peaks at −0.65, −0.70, −1.06, −1.24, −1.61, −1.78, and −1.85 V and one irreversible oxidation peak at +0.77 V (Figure S16). When we compare the redox properties of Zn(II)Pcs **1** and **2** and $Sc_3N@I_h-C_{80}$ derivative **4**, it is possible to conclude that the EMF derivative is both easier to reduce and to oxidize than Zn(II)Pcs **1** and **2**, respectively. In other words, electron transfer from Zn(II)Pc **1** to **4** is theoretically feasible upon complexation. Moreover, a change of the supramolecular "partner" of **4** from Zn(II)Pc **1** to **2** is expected to reverse the direction of the photoinduced charge transfer from the EMF to the electron-accepting, octasulfonyl Zn(II)Pc.

The possible interactions in the ground state between Zn(II)Pcs **1** and **2**, on one hand, and **3** and **4**, on the other hand, were investigated by visible/near-infrared absorption spectroscopy in chlorobenzene and in *o*-DCB. Absorption assays with solutions of Zn(II)Pcs **1** and **2** titrated with variable amounts of **3** and **4** were performed maintaining the total Zn(II)Pc concentration constant at 1.0×10^{-6} M. Absorption changes of the Soret- and Q-band were monitored at 350 and 680 nm for Zn(II)Pc **1** and at 360 and 690 nm for Zn(II)Pc **2**, respectively. However, only in the case of Zn(II)Pc **2** changes in its absorption features were observed upon addition of fullerene derivatives **3** and **4** (Figure 2). Well-defined isosbestic points at 307, 382, 522, and 706 nm for **2**/**3** and at 390 nm for **2**/**4** indicate the formation of Zn(II)Pc/fullerene supra-

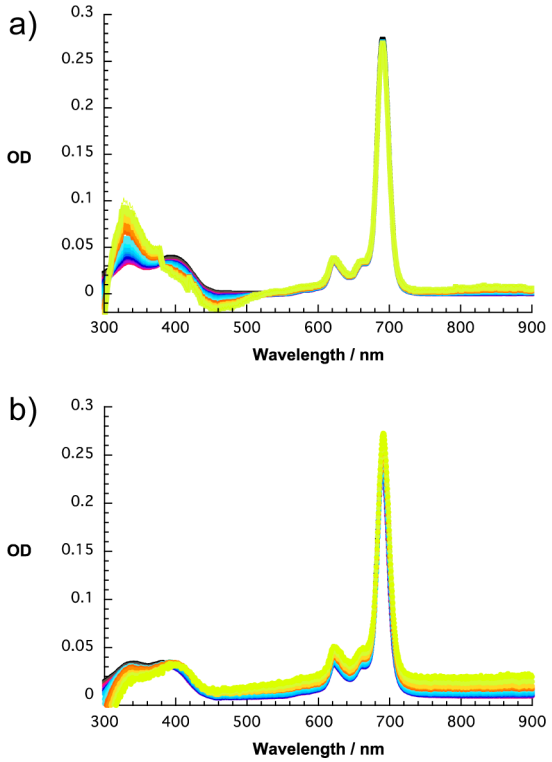

Figure 2. (a) Steady-state absorption spectra of electron-deficient Zn(II)Pc **2** upon addition of C_{60} derivative **3**, from 0 (black spectrum) up to 1.1×10^{-5} M (yellow spectrum) in chlorobenzene at room temperature. (b) Steady-state absorption spectra of electron-deficient Zn(II)Pc **2** upon addition of $Sc_3N@I_h-C_{80}$ derivative **4**, from 0 (black spectrum) up to 1.1×10^{-5} M (yellow spectrum), in chlorobenzene at room temperature. Both in a and b, the total concentration of the Zn(II)Pc during the titration was maintained constant at 1.0×10^{-6} M and the absorption of the added fullerenes were subtracted from the corresponding spectra.

DOI: 10.1021/jacs.5b06454
J. Am. Chem. Soc. 2015, 137, 12914−12922

molecular complexes and appreciable ground-state coupling. A 1:1 stoichiometry for both supramolecular complexes **2**/**3** and **2**/**4** was established by Job plot analysis (Figure S18 and Figure 3, respectively).

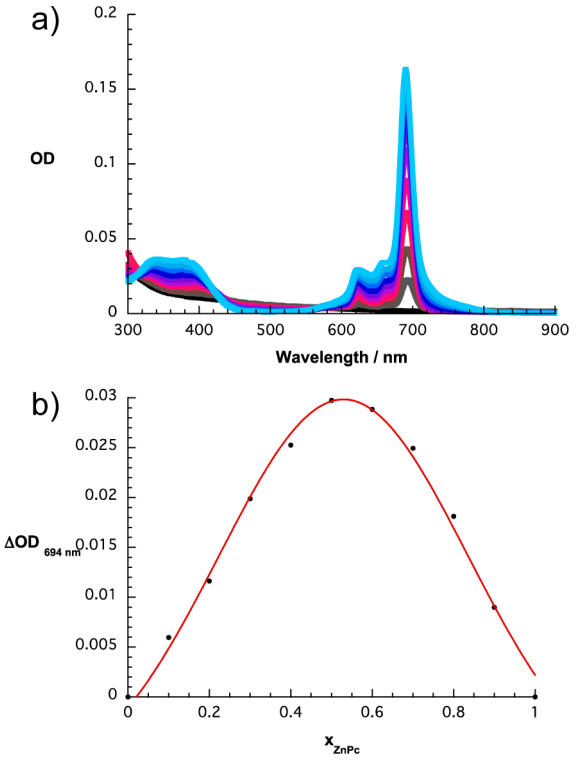

Figure 3. (a) UV−vis absorption spectra obtained at different **2**/**4** ratios from 0 (light blue spectrum) to 1 (black spectrum) at 0.1 increment in chlorobenzene (total concentration = 1.0×10^{-6} M). (b) Job plot analysis for the complexation of electron-deficient Zn(II)Pc **2** with $Sc_3N@I_h$−C_{80} derivative **4** in chlorobenzene monitored at 694 nm.

Insights into the excited-state interactions within the Zn(II)Pc−fullerene supramolecular ensembles were obtained from steady-state fluorescence measurements in chlorobenzene and *o*-DCB. The Zn(II)Pc-centered fluorescence of derivatives **1** and **2** with maxima at 685 and 694 nm, respectively, were monitored upon photoexcitation at either 610 or 630 nm. For both Zn(II)Pcs, an exponential decrease of their fluorescence is observed upon addition of derivative **4** until the end point of the titration is reached (i.e., after the addition of 11 and 6 equiv of **4** to Zn(II)Pcs **1** and **2**, respectively), a change associated with the quantitative formation of the Zn(II)Pc/fullerene hybrids (Figure 4). A similar trend was observed upon replacing **4** for C_{60} derivative **3** (Figures S19, S20). The Zn(II)Pc fluorescence quantum yield in the supramolecular complexes **1**/**3**, **2**/**3**, **1**/**4**, and **2**/**4** is 0.02, 0.08, 0.11, and 0.06, respectively. These values are significantly lower than the 0.30 and 0.23 obtained for uncomplexed Zn(II)Pcs **1** and **2**, respectively. Taking into account a 1:1 complexation stoichiometry between the Zn(II)Pc and the pyridine-substituted fulleropyrrolidine (vide supra), the Zn(II)Pc/fullerene binding constants for the four supramolecular complexes were calculated using the fluorescence titration data according to eq 1

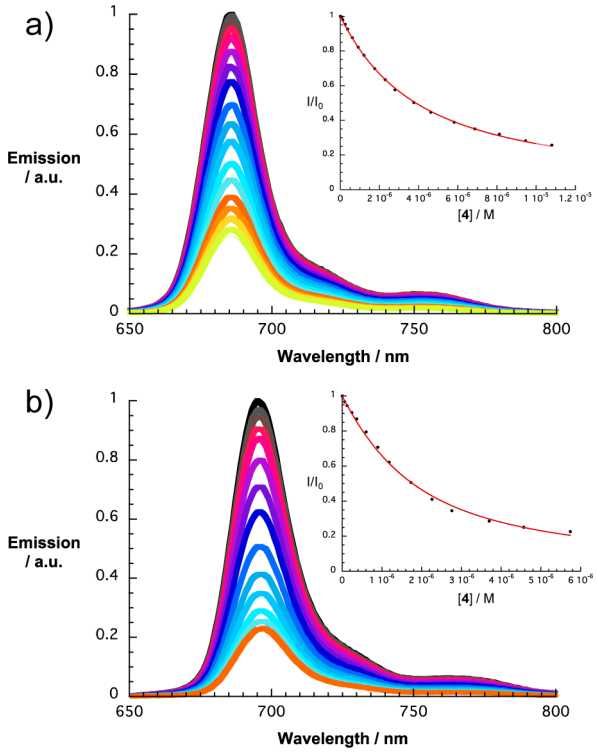

Figure 4. (a) Steady-state fluorescence spectra (λ_{exc} = 610 nm) of electron-rich Zn(II)Pc **1** upon addition of $Sc_3N@I_h$−C_{80} derivative **4** (from 0 (black spectrum) up to 1.1×10^{-5} M (yellow spectrum)) in chlorobenzene at room temperature. Inset: Plot of the change in fluorescence intensity at 685 nm as a ratio of I_F/I_0 versus the concentration of **4**. The solid line shows the curve-fit (with an *R* value of 0.999) obtained by nonlinear least-squares analysis. (b) Steady-state fluorescence spectra (λ_{exc} = 630 nm) of electron-deficient Zn(II)Pc **2** upon addition of $Sc_3N@I_h$−C_{80} derivative **4** (from 0 (black spectrum) up to 5.7×10^{-6} M (yellow spectrum)) in chlorobenzene at room temperature. Inset: Plot of the change in fluorescence intensity at 695 nm as a ratio of I_F/I_0 versus the concentration of **4**. The solid line shows the curve-fit (with an *R* value of 0.997) obtained by nonlinear least-squares analysis. Both in a and b, the total concentration of the Zn(II)Pc during the titration was maintained constant at 1.0×10^{-6} M.

$$\frac{I}{I_0} = 1 - \frac{1}{2c_0}\left[\left(c_F + c_0 + \frac{1}{K_{ass}}\right) - \sqrt{\left(c_F + c_0 + \frac{1}{K_{ass}}\right)^2 - 4c_0c_F}\right] \quad (1)$$

where K_{ass} is the binding constant, c_0 is the concentration of Zn(II)Pc **1** or **2**, and c_F is the concentration of the fullerene derivatives **3** or **4**. Overall, the binding constants, log K_{ass}, were 6.1 ± 0.1 (**1**/**3**), 6.2 ± 0.2 (**2**/**3**), 5.5 ± 0.1 (**1**/**4**), and 5.9 ± 0.1 (**2**/**4**) in chlorobenzene (Figures 4, S18, S20).

Prior to transient absorption measurements, spectroelectrochemical experiments were deemed necessary to assist in the interpretation of the excited-state spectral features of the four supramolecular complexes (vide infra). To this end, the formation of the one-electron reduced form of electron-deficient Zn(II)Pc **2** and the one-electron oxidized forms of electron-rich Zn(II)Pc **1** and $Sc_3N@I_h$−C_{80} derivative **4** were monitored upon spectroelectrochemical reduction and oxida-

DOI: 10.1021/jacs.5b06454
J. Am. Chem. Soc. 2015, 137, 12914−12922

tion, respectively, in deaerated *o*-DCB. The differential absorption spectrum of Zn(II)Pc **2** upon spectroelectrochemical reduction displays sets of maxima at 476, 605, 647, 769, 960, and 1100 nm, as well as minima at 426, 628, 665, and 695 nm (Figure 5a). On the other hand, spectroelectrochemistry of

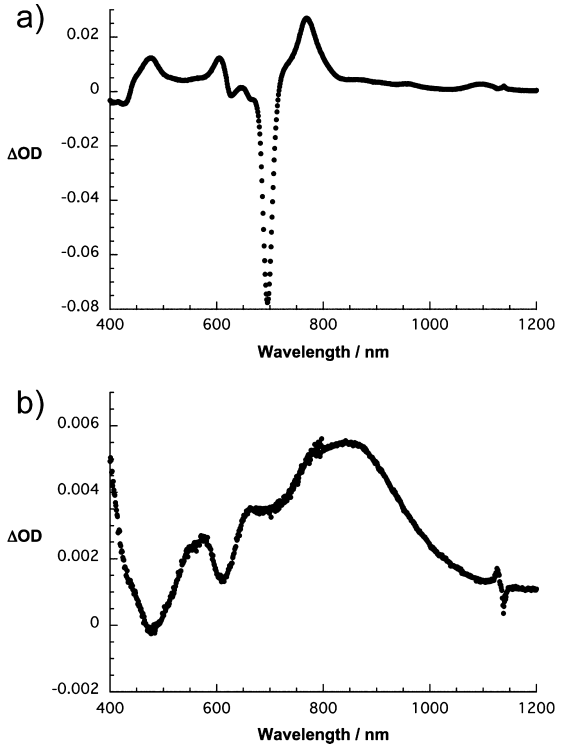

Figure 5. Differential absorption spectra (visible and near-infrared) obtained upon (a) electrochemical reduction of electron-deficient Zn(II)Pc **2** (applied bias of −0.8 V) and (b) electrochemical oxidation of $Sc_3N@I_h$–C_{80} derivative **4** (applied bias of +0.8 V) in argon-saturated *o*-DCB at room temperature with 0.05 M *n*-Bu_4NPF_6 as supporting electrolyte and silver-wire as pseudoreference electrode.

Zn(II)Pc **1** under oxidative conditions (Figure S21) reveals differential absorption maxima at 442, 528, 728, and 836 nm as well as minima at 613, 650, and 680 nm. Similarly, spectroelectrochemical oxidation of $Sc_3N@I_h$–C_{80} derivative **4** shows differential absorption changes that include maxima at 715 and 880 nm and a broad tail that reaches out into the near-infrared region (Figure 5b). On the other hand, the absorption features of the reduced $Sc_3N@I_h$–C_{80} derivative **4** were obtained by pulse radiolytic studies which led to differential absorption spectra with a maximum at 830 nm and a broad near-infrared tail (Figure S22).[7e] The radical anion of C_{60} derivative **3** reveals a characteristic maximum at 1010 nm upon pulse radiolytic reduction.[2b,24]

Insights about the formation, and decay, of photogenerated charge separated species for hybrids **1**/**3**, **2**/**3**, **1**/**4**, and **2**/**4** were derived from transient absorption studies following femtosecond and nanosecond excitation. The differential absorption spectra in our time-resolved experiments were calculated according to eq 2,

$$\Delta OD(\lambda, \Delta t) = -\log\left(\frac{I_{ex}(\lambda, \Delta t)}{I_0(\lambda)}\right) \quad (2)$$

where I_{ex} and I_0 are the transmitted probe light through the excited and the unexcited sample, respectively. Differential absorption spectra obtained from steady-state experiments, such as titration assays and spectroelectrochemistry, are the simple subtraction of the final spectrum from the initial spectrum. A qualitative comparison between the spectroelectrochemical data and the transient absorption spectra is based on identifying the transients of the radical ion pairs (vide infra).

Compounds **1**–**4** were individually investigated. Upon excitation of C_{60} derivative **3** with a 387 nm laser pulse (Figure S26), differential absorption spectra arise, which are attributed to the population of the singlet excited state of C_{60} with characteristic absorption maxima in the visible at 520 nm and in the near-infrared between 800 and 1200 nm. The C_{60} singlet excited state features undergo quantitative intersystem crossing with a lifetime of 1.5 ± 0.1 ns to afford its triplet manifold with a characteristic maximum at 700 nm and a lifetime up to 20 μs in oxygen-free chlorobenzene. Photoexcitation of a chlorobenzene solution of $Sc_3N@I_h$–C_{80} derivative **4** with a 387 nm laser pulse (Figure S27) leads to differential absorption changes that include strong transient maxima at 480 and 1025 nm. The singlet excited state features of **4** decay fast with a lifetime of 25 ± 5 ps. The presence of the C_{80}-encapsulated Sc_3N cluster in **4** is likely to be responsible for the fast singlet excited state decay to yield the triplet manifold. Turning to Zn(II)Pcs, **1** (Figures S23 and S24) reveals differential absorption changes that include transient maxima at 483, 598, 638, 739, and 825 nm, as well as transient minima at 615 and 683 nm upon excitation at 676 nm. These transients correlate with the singlet excited state of Zn(II)Pc **1** and have an intrinsic lifetime of 2.8 ± 0.1 ns in chlorobenzene. In **1**, the singlet–singlet transitions undergo intersystem crossing to the corresponding triplet excited state with a transient maximum at 500 nm and transient minima at 615, 652, and 682 nm. For the chlorobenzene solution of sulfonyl-substituted Zn(II)Pc **2**, it was necessary to add small amounts of pyridine to circumvent Zn(II)Pc aggregation, which otherwise dominates the outcome of the femtosecond transient absorption experiments even at Zn(II)Pc concentrations as low as 1×10^{-5} M. The differential absorption spectra of **2** (Figure S25) reveal transient maxima at 521, 647, and 850 nm as well as transient minima at 624 and 695 nm upon 676 nm laser irradiation. Similar to Zn(II)Pc **1**, we ascribe these differential absorption changes to the formation of the singlet excited state of **2**, which undergoes intersystem crossing with a time constant of 2.8 ± 0.1 ns to form the corresponding triplet excited state. The triplet excited state displays characteristic transient absorption maxima at 440 and 810 nm and minima at 624, 664, and 694 nm.

Next, transient absorption analysis of supramolecular complexes **1**/**3**, **2**/**3**, **1**/**4**, and **2**/**4** was carried out. Differential absorption spectra of hybrid **1**/**3** include transient maxima at 495, 600, 640, and 800 nm and minima at 616 and 680 nm which were observed directly after photoexcitation with 676 nm laser pulses (Figures S28 and S29). These transient features relate to the singlet excited state features of Zn(II)Pc **1** (vide supra). In contrast to **1**, in supramolecular ensemble **1**/**3** these features decay within 29 ± 1 ps and give rise to new transient maxima at 540, 720, 850, and 1024 nm as well as to transient minima at 617 and 680 nm. These features, especially those in the near-infrared, are reliable fingerprints of the one-electron oxidized Zn(II)Pc **1** and the one-electron reduced fullerene **3** species,[2b,24] that is, $\mathbf{1}^{\bullet+}/\mathbf{3}^{\bullet-}$. From a multiwavelength kinetic analysis, a lifetime of 9.0 ± 0.5 ns in chlorobenzene was deduced for the $\mathbf{1}^{\bullet+}/\mathbf{3}^{\bullet-}$ radical ion pair state. Notably, the product of charge recombination is the triplet excited state of

DOI: 10.1021/jacs.5b06454
J. Am. Chem. Soc. 2015, 137, 12914–12922

electron-rich Zn(II)Pc **1**. Photoexcitation of supramolecular hybrid **2**/**3** with 676 nm laser pulses leads to the exclusive population of the singlet excited state of electron-deficient Zn(II)Pc **2** with transient maxima at 521, 647, and 850 nm and minima at 624 and 695 nm (Figure S25), in agreement with the transient absorption experiments of **2** (vide supra). These latter transitions then decay to the corresponding triplet excited state features of **2** with maxima at 445, 647, and 810 nm and minima at 624, 664, and 693 nm, similar to what was observed for uncomplexed Zn(II)Pc **2**. In the case of supramolecular complex **2**/**3** no evidence for any PET event is observed. An electron transfer from the singlet excited state of Zn(II)Pc **2**, with an energy of 1.79 eV, to C_{60} derivative **3** is ruled out on thermodynamic grounds due to the high radical ion pair state energy for $\mathbf{2}^{\bullet+}/\mathbf{3}^{\bullet-}$. From electrochemical experiments performed with the individual components **2** and **3**, a $\mathbf{2}^{\bullet+}/\mathbf{3}^{\bullet-}$ radical ion pair state energy of 1.89 eV was calculated. Notably, axial coordination of pyridyl derivatives to Zn(II)Pc **2** is known to shift the oxidation potential by ~0.2 eV.[25] In other words, electron transfer from the electron-accepting Zn(II)Pc **2** singlet excited state to the C_{60} derivative **3** is energetically unfavorable.

Laser irradiation of D−A hybrid **1**/**4** at 676 nm leads to transient absorption spectra with maxima at 500, 600, 640, 739, and 825 nm and minima at 615 and 683 nm (Figure 6). Overall, these features confirm the successful formation of the singlet excited state species of Zn(II)Pc **1**, which is located at 1.82 eV. With a lifetime of 6.8 ± 0.5 ps, these features decay giving rise to new transients with maxima at 440, 512, and 850 nm and minima at 615 and 683 nm. This result is indicative of the formation of the one-electron oxidized Zn(II)Pc **1**, in agreement with the spectroelectrochemical oxidation features of Zn(II)Pc **1** (Figure S21). On the other hand, evidence of the formation of $\mathbf{4}^{\bullet-}$ is based on the broad near-infrared tail observed.[7e] Overall, these changes in transient absorptions of **1**/**4** can be assigned to a charge transfer from the electron-donating Zn(II)Pc **1** to the electron-accepting $Sc_3N@I_h$−C_{80} **4** to form the $\mathbf{1}^{\bullet+}/\mathbf{4}^{\bullet-}$ radical ion pair state with energy of 1.20 eV. The superimposed features of $\mathbf{1}^{\bullet+}$ and $\mathbf{4}^{\bullet-}$ are in sound agreement with those recorded for the $\mathbf{1}^{\bullet+}/\mathbf{4}^{\bullet-}$ radical ion pair (Figure 6c). The latter radical ion pair state consequently undergoes charge recombination within 180 ± 10 ps to the singlet ground state of Zn(II)Pc **1** (Figure 8a). At the conclusion of the 8 ns time scale, the triplet excited state of Zn(II)Pc is detected, whose formation is connected to a minor extend to charge recombination and to a major extend to regular intersystem crossing in uncomplexed Zn(II)Pc **1**. Notably, the $\mathbf{1}^{\bullet-}/\mathbf{4}^{\bullet+}$ radical ion pair state is nearly isoenergetic with the singlet excited state of **1**, so basically without any thermodynamic driving force, as such a charge transfer, with presumably a reasonable activation barrier, might be feasible by thermal activation. This process is, however, placed deep in the Marcus normal region and, thus, not competitive with the ultrafast charge separation that gives the $\mathbf{1}^{\bullet+}/\mathbf{4}^{\bullet-}$ radical ion pair state.

Finally, supramolecular ensemble **2**/**4** was probed and the differential absorption spectra were recorded (Figure 7). Upon 676 nm laser excitation, transient absorption maxima at 522, 647, and 850 nm and minima at 624 and 695 nm corroborate the population of the singlet excited state of Zn(II)Pc **2**. This singlet excited state decays rapidly with a lifetime of 6.6 ± 0.1 ps, followed by the formation of new maxima at 465, 603, 646, 760, and 1060 nm and minima at 625 and 695 nm. From a

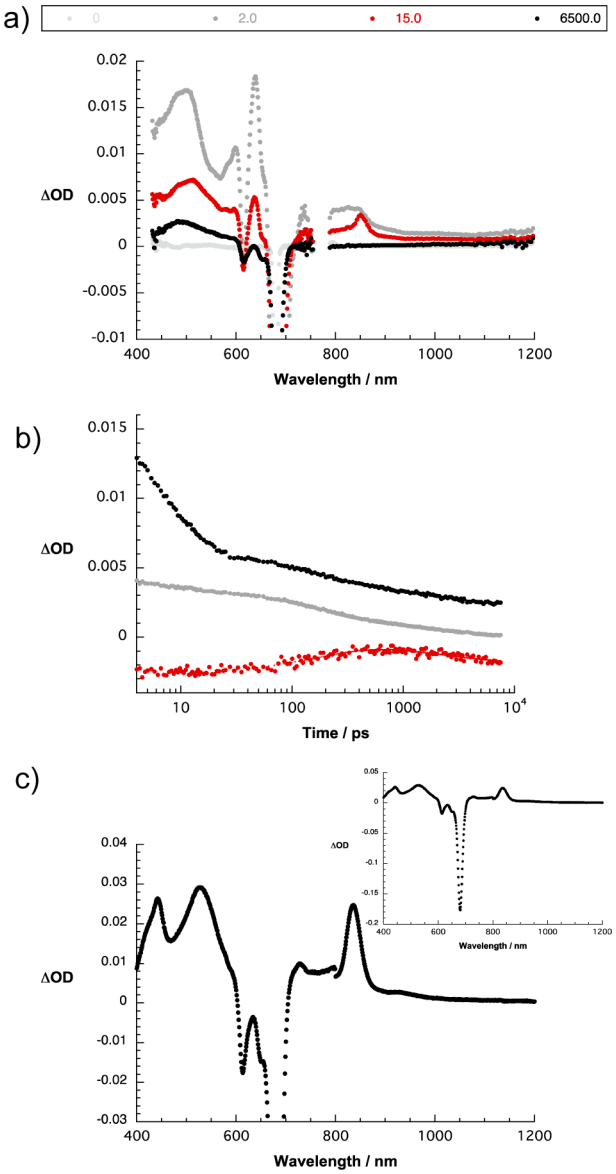

Figure 6. (a) Differential absorption spectra (visible and near-infrared) obtained upon femtosecond flash photolysis (676 nm) of supramolecular ensemble **1**/**4** ([**1**] = 1 × 10^{-5} M, ratio between **4** and **1** = 10) in argon-saturated chlorobenzene with several time delays of 0 ps (ground state), 2 ps (singlet excited state), 15 ps (radical ion pair state), and 6500 ps (triplet excited state). (b) Time-absorption profiles of the spectra shown above at 515 nm (black), 615 nm (red), and 850 nm (gray) monitoring the charge separation (6.8 ± 0.5 ps) and the charge recombination (180 ± 10 ps) kinetics. (c) Superimposed differential absorption spectra (visible and near-infrared) of $\mathbf{1}^{\bullet+}$ and $\mathbf{4}^{\bullet-}$; inset shows the full *y*-scale.

comparison of these transient spectra with the spectrum obtained from the spectroelectrochemical reduction of **2** (Figure 5a), it is possible to assign the visible bands in the former spectra to the one-electron reduced form of Zn(II)Pc **2**, namely $\mathbf{2}^{\bullet-}$.[26] On the other hand, the features of the $Sc_3N@I_h$−C_{80} derivative **4** radical cation species, namely $\mathbf{4}^{\bullet+}$, could also be identified by comparison with the spectrum obtained upon spectroelectrochemical oxidation of **4** (Figure 5b). In accordance with these results, and differently from ensemble **1**/**4**, a PET process from the electron-donating $Sc_3N@I_h$−C_{80} **4** to the photoexcited electron-accepting Zn(II)Pc **2** must be

DOI: 10.1021/jacs.5b06454
J. Am. Chem. Soc. 2015, 137, 12914−12922

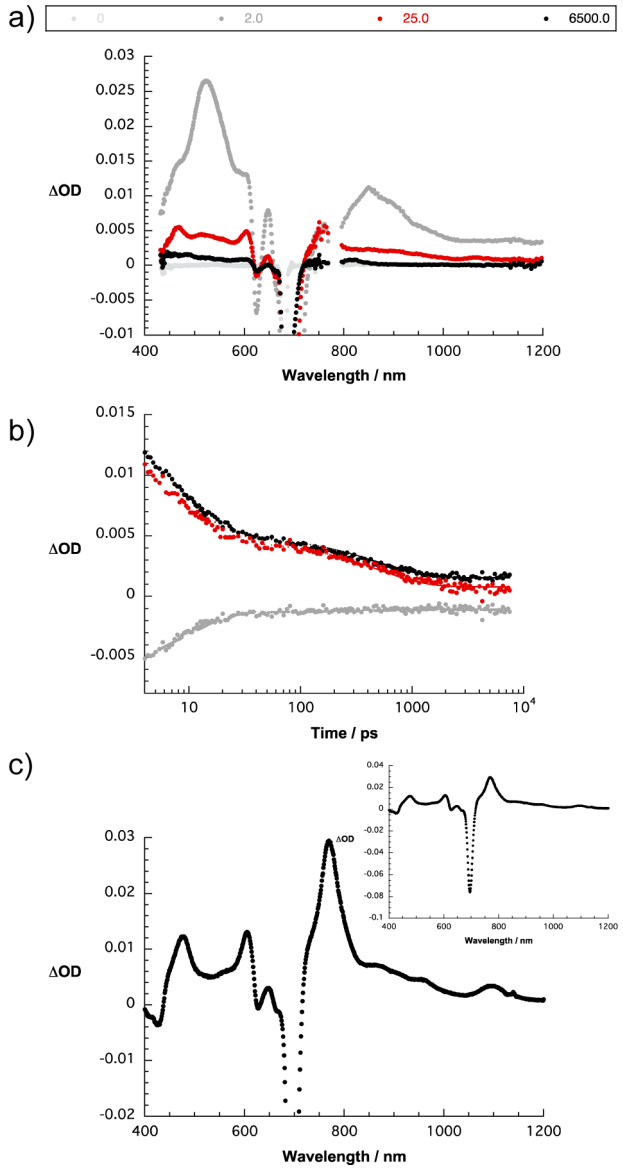

Figure 7. (a) Differential absorption spectra (visible and near-infrared) obtained upon femtosecond flash photolysis (676 nm) of supramolecular ensemble **2**/**4** ([**2**] = 1 × 10^{-5} M, ratio between **4** and **2** = 10) in argon-saturated chlorobenzene with several time delays of 0 ps (ground state), 2 ps (singlet excited state), 25 ps (radical ion pair state), and 6500 ps (ground state) at room temperature. (b) Time-absorption profiles of the spectra shown above at 465 nm (black), 604 nm (red), and 624 nm (gray) monitoring the charge separation (6.6 ± 0.1 ps) and the charge recombination (505 ± 10) processes. (c) Superimposed differential absorption spectra (visible and near-infrared) of $\mathbf{2}^{\bullet-}$ and $\mathbf{4}^{\bullet+}$; inset shows the full y-scale.

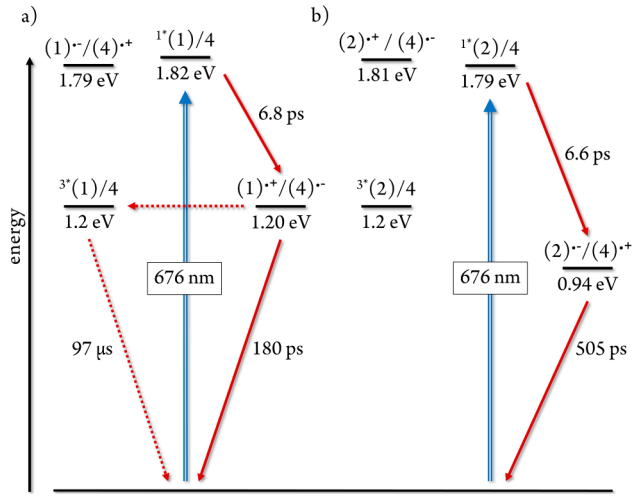

Figure 8. Energy level diagrams for supramolecular ensembles (a) **1**/**4** and (b) **2**/**4** in chlorobenzene reflecting major (solid arrows) and minor (dashed arrows) energetic pathways of charge separation and charge recombination.[27] The energy of the $\mathbf{1}^{\bullet+}/\mathbf{4}^{\bullet-}$ and $\mathbf{2}^{\bullet-}/\mathbf{4}^{\bullet+}$ radical ion pairs were derived by the simple addition of the corresponding redox potentials, that is, oxidation of **1**/reduction of **4** and reduction of **2**/oxidation of **4**.

occurring to yield the $\mathbf{2}^{\bullet-}/\mathbf{4}^{\bullet+}$ radical ion pair state at 0.94 eV instead of the energetically unfavorable uphill $\mathbf{2}^{\bullet+}/\mathbf{4}^{\bullet-}$ species at 1.81 eV. Notably, the superimposed features of $\mathbf{2}^{\bullet-}$ and $\mathbf{4}^{\bullet+}$ are in sound agreement with those recorded for the $\mathbf{2}^{\bullet-}/\mathbf{4}^{\bullet+}$ radical ion pair (Figure 7c). The photogenerated $\mathbf{2}^{\bullet-}/\mathbf{4}^{\bullet+}$ charge separated state, which has a lifetime of 505 ± 10 ps in chlorobenzene, then recombines to give rise to the ground state of Zn(II)Pc **2** (Figure 8b).

From the time-resolved absorption assays, it is possible to conclude that Zn(II)Pc-to-fullerene and fullerene-to-Zn(II)Pc electron transfer dictates the excited state deactivation in supramolecular complexes **1**/**3** and **1**/**4** (Pc-to-fullerene), and **2**/**4** (fullerene-to-Pc), while in **2**/**3**, no evidence for an electron transfer was observed. Moreover, in Zn(II)Pc/$Sc_3N@I_h$–C_{80} hybrids **1**/**4** and **2**/**4**, charge separation is accelerated by an order of magnitude relative to the C_{60} hybrid **1**/**3**, 1.5 × 10^{11} vs 3.4 × 10^{10} s^{-1}. Nevertheless, the Zn(II)Pc/C_{60} hybrid **1**/**3** outperforms both Zn(II)Pc/$Sc_3N@I_h$–C_{80} hybrids **1**/**4** and **2**/**4** in terms of charge separated state lifetime by 1 order of magnitude as inferred by analyses of the transient absorption measurements which afforded charge recombination rate constants of 1.1 × 10^8, 5.6 × 10^9, and 2.0 × 10^9 s^{-1} for complexes **1**/**3**, **1**/**4**, and **2**/**4**, respectively.

CONCLUSION

We have successfully prepared four electron D–A ensembles built on metal–ligand coordination between C_{60} or $Sc_3N@I_h$–C_{80} featuring a pyridyl moiety, on one hand, and electron-donating or electron-accepting Zn(II)Pcs, on the other hand. Interestingly, full-fledged photophysical assays with those two ensembles that contain $Sc_3N@I_h$–C_{80} **4** axially coordinate either to the electron-donating Zn(II)Pc **1** or to the electron-accepting Zn(II)Pc **2** revealed a switchable electron transfer reactivity. Spectroscopic and kinetic evidence for a Zn(II)Pc-to-$Sc_3N@I_h$–C_{80} as well as $Sc_3N@I_h$–C_{80}-to-Zn(II)Pc electron transfer, upon light excitation, was established as the major deactivation pathways in time-resolved pump probe experiments. This is, to the best of our knowledge, the first time that a fullerene-based molecular building block shows an electron transfer dualism, namely acting both as electron-acceptor or electron-donor. Its outcome is simply governed by the electronic nature of its counterpart. This finding, in combination with the small reorganization energy of fullerenes in electron transfer reactions, is likely to pave the road to the preparation of novel switching devices, solar energy conversion schemes, and logic gates based on $Sc_3N@I_h$–C_{80}, one of the most abundant and easy-to-purify fullerene. Particularly interesting is also the use of self-assembly *en-route* toward the

DOI: 10.1021/jacs.5b06454
J. Am. Chem. Soc. 2015, 137, 12914–12922

preparation and study of a plethora of easy-to-prepare D−A constructs showing switchable electron transfer features.

■ ASSOCIATED CONTENT

Supporting Information

The Supporting Information is available free of charge on the ACS Publications website at DOI: 10.1021/jacs.5b06454.

Experimental details including the synthetic procedures leading to compounds **1**−**4**, HPLC profiles, 1D- and 2D-NMR spectra, mass spectra, UV−vis spectra, DPV curves, femtosecond transient absorption spectra, and spectroelectrochemical spectra (PDF)

■ AUTHOR INFORMATION

Corresponding Authors

*dirk.guldi@fau.de
*tomas.torres@uam.es
*akaska@tara.tsukuba.ac.jp
* echegoyen@utep.edu

Notes

The authors declare no competing financial interest.

■ ACKNOWLEDGMENTS

Financial support from Deutsche Forschungsgemeinschaft, the MICINN, Spain (CTQ- 2014-52869-P), the Comunidad de Madrid (S2013/MIT-2841 FOTOCARBON) and the EU ("SO2S" FP7-PEOPLE-2012-ITN, No.: 316975) is acknowledged. L.E. wishes to thank the U.S. National Science Foundation, Grants DMR-1205302 PREM Program and CHE-1408865, as well as the Robert A. Welch Foundation for an endowed chair, Grant No. AH-0033, for generous financial support.

■ REFERENCES

(1) (a) Scholes, G. D.; Fleming, G. R.; Olaya-Castro, A.; van Grondelle, R. *Nat. Chem.* **2011**, *3*, 763−774. (b) Cogdell, R. J.; Brotosudarmo, T. H. P.; Gardiner, A. T.; Sanchez, P. M.; Cronin, L. *Biofuels* **2010**, *1*, 861−876. (c) Special issue on "Artificial Photosynthesis and Solar Fuels". *Acc. Chem. Res.* **2009**, *42*, 1859−2029.

(2) (a) Guldi, D. M. *Chem. Soc. Rev.* **2002**, *31*, 22−36. (b) Guldi, D. M.; Prato, M. *Acc. Chem. Res.* **2000**, *33*, 695−703.

(3) (a) Clarke, T. M.; Durrant, J. R. *Chem. Rev.* **2010**, *110*, 6736−6767. (b) *Fullerenes: Principles and Applications*; Langa, F., Nierengarten, J.-F.; Eds.; Nanoscience and Nanotechnology Series; The Royal Society of Chemistry: Cambridge, U.K., 2007. (c) *Fullerenes: From Synthesis to Optoelectronic Properties*; Guldi, D. M., Martin, N., Eds.; Kluwer Academic Publishers: Dodrecht, The Netherlands, 2002. (d) Kamat, P. V. *J. Phys. Chem. C* **2007**, *111*, 2834−2860.

(4) (a) Maroto, E. E.; Izquierdo, M.; Reboredo, S.; Marco-Martínez, J.; Filippone, S.; Martín, N. *Acc. Chem. Res.* **2014**, *47*, 2660−2670. (b) Zhu, S.-E.; Li, F.; Wang, G.-W. *Chem. Soc. Rev.* **2013**, *42*, 7535−7570. (c) Prato, M.; Maggini, M. *Acc. Chem. Res.* **1998**, *31*, 519−526.

(5) (a) Ohkubo, K.; Ortiz, J.; Martin-Gomis, L.; Fernandez-Lazaro, F.; Sastre-Santos, A.; Fukuzumi, S. *Chem. Commun.* **2007**, 589−591. (b) Rudolf, M.; Trukhina, O.; Perles, J.; Feng, L.; Akasaka, T.; Torres, T.; Guldi, D. M. *Chem. Sci.* **2015**, *6*, 4141−4147.

(6) (a) Wang, T.; Wang, Ch. *Acc. Chem. Res.* **2014**, *47*, 450−458. (b) Cong, H.; Yu, B.; Akasaka, T.; Lu, X. *Coord. Chem. Rev.* **2013**, *257*, 2880−2898. (c) Popov, A. A.; Yang, S.; Dunsch, L. *Chem. Rev.* **2013**, *113*, 5989−6113. (d) Zhang, J.; Stevenson, S.; Dorn, H. C. *Acc. Chem. Res.* **2013**, *46*, 1548−1557.

(7) (a) Liu, B.; Fang, H.; Li, X.; Cai, W.; Bao, L.; Rudolf, M.; Plass, F.; Fan, L.; Lu, X.; Guldi, D. M. *Chem. - Eur. J.* **2015**, *21*, 746−752. (b) Takano, Y.; Herranz, M. Á.; Martín, N.; Radhakrishnan, S. G.; Guldi, D. M.; Tsuchiya, T.; Nagase, S.; Akasaka, T. *J. Am. Chem. Soc.* **2010**, *132*, 8048−8055. (c) Ross, R. B.; Cardona, C. M.; Guldi, D. M.; Gayathri, S. S.; Reese, M. O.; Kopidakis, N.; Peet, J.; Walker, B.; Bazan, G. C.; Van Keuren, E.; Holloway, B. C.; Drees, M. *Nat. Mater.* **2009**, *8*, 208−212. (d) Pinzon, J. R.; Gasca, D. C.; Gayathri, S. S.; Bottari, G.; Torres, T.; Guldi, D. M.; Echegoyen, L. *J. Am. Chem. Soc.* **2009**, *131*, 7727−7734. (e) Pinzon, J. R.; Cardona, C. M.; Herranz, M. A.; Plonska-Brzezinska, M. E.; Palkar, A.; Athans, A. J.; Martin, N.; Rodriguez-Fortea, A.; Poblet, J. M.; Bottari, G.; Torres, T.; Gayathri, S. S.; Guldi, D. M.; Echegoyen, L. *Chem. - Eur. J.* **2009**, *15*, 864−877.

(8) (a) Feng, L.; Rudolf, M.; Trukhina, O.; Slanina, Z.; Uhlik, F.; Lu, X.; Torres, T.; Guldi, D. M.; Akasaka, T. *Chem. Commun.* **2015**, *51*, 330−333. (b) Rudolf, M.; Feng, L.; Slanina, Z.; Akasaka, T.; Nagase, S.; Guldi, D. M. *J. Am. Chem. Soc.* **2013**, *135*, 11165−11174. (c) Feng, L.; Rudolf, M.; Wolfrum, S.; Troeger, A.; Slanina, Z.; Akasaka, T.; Nagase, S.; Martín, N.; Ameri, N. T.; Brabec, C. J.; Guldi, D. M. *J. Am. Chem. Soc.* **2012**, *134*, 12190−12197. (d) Takano, Y.; Obuchi, S.; Mizorogi, N.; García, R.; Herranz, M. A.; Rudolf, M.; Guldi, D. M.; Martín, N.; Nagase, S.; Akasaka, T. *J. Am. Chem. Soc.* **2012**, *134*, 19401−19408.

(9) (a) Tsuchiya, T.; Rudolf, M.; Wolfrum, S.; Gayathri, S. R.; Aoyama, R.; Yokosawa, Y.; Oshima, A.; Akasaka, T.; Nagase, S.; Guldi, D. M. *Chem. - Eur. J.* **2013**, *19*, 558−565. (b) Kamimura, T.; Ohkubo, K.; Kawashima, Y.; Nobukuni, H.; Naruta, Y.; Tani, F.; Fukuzumi, S. *Chem. Sci.* **2013**, *4*, 1451−1461. (c) Grimm, B.; Schornbaum, J.; Cardona, C. M.; van Paauwe, J. D.; Boyd, P. D. W.; Guldi, D. M. *Chem. Sci.* **2011**, *2*, 1530−1537.

(10) Ohkubo, K.; Mase, K.; Karnas, E.; Sessler, J. L.; Fukuzumi, S. *J. Phys. Chem. C* **2014**, *118*, 18436−18444.

(11) *Handbook of Porphyrin Science*; Kadish, K. M., Smith, K. M., Guilard, R., Eds.; Academic Press: San Diego, CA, 2010; Vols. *1*−*15*.

(12) (a) Bottari, G.; de la Torre, G.; Torres, T. *Acc. Chem. Res.* **2015**, *48*, 900−910. (b) Bill, N. L.; Trukhina, O.; Sessler, J. L.; Torres, T. *Chem. Commun.* **2015**, *51*, 7781−7794. (c) Bottari, G.; Trukhina, O.; Ince, M.; Torres, T. *Coord. Chem. Rev.* **2012**, *256*, 2453−2477. (d) Bottari, G.; de la Torre, G.; Guldi, D. M.; Torres, T. *Chem. Rev.* **2010**, *110*, 6768−6816. (e) D'Souza, F.; Ito, O. *Coord. Chem. Rev.* **2005**, *249*, 1410−1422.

(13) (a) Stevenson, S.; Mackey, M. A.; Thompson, M. C.; Coumbe, H. L.; Madasu, P. K.; Coumbe, C. E.; Phillips, J. P. *Chem. Commun.* **2007**, *41*, 4263−4265. (b) Stevenson, S.; Thompson, M. C.; Coumbe, H. L.; Mackey, M. A.; Coumbe, C. E.; Phillips, J. P. *J. Am. Chem. Soc.* **2007**, *129*, 16257−16262.

(14) (a) Stevenson, S.; Mackey, M. A.; Coumbe, C. E.; Phillips, J. P.; Elliott, B.; Echegoyen, L. *J. Am. Chem. Soc.* **2007**, *129*, 6072−6073. (b) Stevenson, S.; Harich, K.; Yu, H.; Stephen, R. R.; Heaps, D.; Coumbe, C.; Phillips, J. P. *J. Am. Chem. Soc.* **2006**, *128*, 8829−8835. (c) Ge, Z.; Duchamp, J. C.; Cai, T.; Gibson, H. W.; Dorn, H. C. *J. Am. Chem. Soc.* **2005**, *127*, 16292−16298. (d) Elliott, B.; Yu, L.; Echegoyen, L. *J. Am. Chem. Soc.* **2005**, *127*, 10885−10888.

(15) Kratschmer, W.; Lamb, L. D.; Fostiropoulos, K.; Huffman, D. R. *Nature* **1990**, *347*, 354−358.

(16) Tat, F. T.; Zhou, Zh.; MacMahon, S.; Song, F.; Rheingold, A. L.; Echegoyen, L.; Schuster, D. I.; Wilson, S. R. *J. Org. Chem.* **2004**, *69*, 4602−4606.

(17) The ratio between the [5,6]- and the [6,6]-$Sc_3N@I_h$−C_{80} adducts was calculated by comparing the areas of their respective HPLC peaks assuming identical absorption coefficients for both fullerene isomers.

(18) Although the isolation of the [6,6]-adduct of $Sc_3N@I_h$−C_{80} derivative **4** was not pursued (it would have implied to stop the reaction at early reaction times (i.e., after 30 min) when the progress of the Prato reaction is still extremely low in order to have the ratio between the [6,6] kinetic product and the [5,6] thermodynamic product at its maximum), its formation was unequivocally determined by ^{1}H- (Figure S8), COSY- (Figure S10) and HSQC- (Figure S11) NMR experiments using a 25:75 mixture of the [6,6]-/[5,6]-$Sc_3N@I_h$−C_{80} isomers.

DOI: 10.1021/jacs.5b06454
J. Am. Chem. Soc. 2015, 137, 12914−12922

(19) Cai, T.; Slebodnick, C.; Xu, L.; Harich, K.; Glass, T. E.; Chancellor, C.; Fettinger, J. C.; Olmstead, M. M.; Balch, A. L.; Gibson, H. W.; Dorn, H. C. *J. Am. Chem. Soc.* **2006**, *128*, 6486−6492.
(20) The formation of $Sc_3N@I_h-C_{80}$ bisadducts, rarely observed in $Sc_3N@I_h-C_{80}$ chemistry due to the poor reactivity of this EMF towards the 1,3-dipolar cycloaddition, was confirmed by a MALDI-TOF peak at 1349.0 *m*/*z* corresponding to the $[C_{94}H_{16}N_5Sc_3]^-$ molecular ion (Figure S4). Considering the high thermal stability of the [6,6]-monoadduct, this observation agrees with recent results reported by Aroua, S. *J. Am. Chem. Soc.* **2015**, *137*, 58−61.
(21) In the case of the [6,6]-adduct, and differently from the [5,6]-adduct, the two methylene protons of the pyrrolidine ring at 4.28 and 3.97 ppm correlate to two magnetically nonequivalent methylene carbon atoms of the pyrrolidine ring at 56.5 and 66.2 ppm, respectively (Figures S11, S12).
(22) Cai, T.; Ge, Zh.; Iezzi, E. B.; Glass, T. E.; Harich, K.; Gibson, H. W.; Dorn, H. C. *Chem. Commun.* **2005**, 3594−3596.
(23) Cardona, C. M.; Elliott, B.; Echegoyen, L. *J. Am. Chem. Soc.* **2006**, *128*, 6480−6485.
(24) Guldi, D. M.; Maggini, M. *Gazz. Chim. Ital.* **1997**, *127*, 779−785.
(25) Kadish, K. M., Smith, K. M., Guilard, R. *The Porphyrin Handbook*; Academic Press: Amsterdam, 2003.
(26) Due to the ratio of approximately 56:1 in terms of extinction coefficients between the 760 nm maximum of $\mathbf{2}^{\bullet-}$ and the 880 nm maximum of $\mathbf{4}^{\bullet+}$, it was not possible, with our instrumental setup, to observe any meaningful contribution from the radical cation signature of $Sc_3N@Ih-C_{80}$ in the differential absorption spectra.
(27) In the case of ensemble **1**/**4**, a competition between radical ion pair deactivation to the singlet ground state as the main pathway, on one hand, and to the triplet excited state of the Zn(II)*Pc* as the minor pathway, on the other hand, without thermodynamic driving force could also possibly occur. The Zn(II)*Pc* triplet excited state features observed in the transient absorption measurements of **2**/**4** likely result from uncomplexed Zn(II)*Pc* **2** in solution.

DOI: 10.1021/jacs.5b06454
J. Am. Chem. Soc. 2015, 137, 12914−12922